Endwall blade profile contouring on wave energy harvesting Impulse turbine

Gautam Maurya, Rishav Raj, Aravind George, Dhiman Chatterjee, Abdus Samad

Abstract— **An oscillating water column (OWC) based wave energy converter incorporates a self-rectifying bidirectional airflow turbine (BDI), which runs in a single direction irrespective of the flow direction. A 0.3m diameter impulse turbine is modelled and meshed in Ansys-ICEMCFD. In this work, commercial computational fluid dynamics (CFD) software was used to predict the performance of an impulse turbine and the effect of the endwall blade profile contouring on the bidirectional impulse turbine is discussed. The detailed flow physics of the turbine with endwall contouring has been presented. It was found that at different fillet radii the flow separation started over the blade suction surface (SS) due to the adverse pressure gradient. The secondary flow losses near the leading edge (LE) reduces due to the shifting of circulating flow structures towards the downstream of the rotor blade. The overall performance was decreased due to pressure drop in downstream guide vane (DGV) and losses occurring near the fillet radii.**

Keywords—**Oscillating water column, Bidirectional turbine, Computational fluid dynamics, Leading edge, Downstream guide vane.**

I. INTRODUCTION

THE modern world is facing energy crisis due to the overexploitation of natural resources. The emerging technologies involved in harnessing the energy from a renewable form of energy are wind, water, solar etc. The ocean is one of the forms of a renewable source of energy, stores an enormous amount of energy in the form of the waves, currents and tide respectively [1]. OWCs (Fig. 1) are the most widely used devices, integrated with air turbines, for the extraction of the wave energy from waves by converting the low pneumatic pressure energy to mechanical energy and further to electrical energy by a generator [2]. There are various types of turbines used for the extraction of wave energy, and among them, the

Paper ID: 1354, Conference Track: Wave device development and testing.

G. Maurya, R. Raj, A. George and A. Samad are with the Wave Energy and Fluids Engineering Lab, Department of Ocean Engineering, IIT Madras, Chennai 600036, Tamil Nadu, India (emails: gtmaur@gmail.com, rishavrajrnc@gmail.com, georgejr.mechengg@gmail.com, samad@iitm.ac.in)

D. Chatterjee is with the Turbomachines Laboratory, Mechanical Engineering Department, IIT Madras, Chennai 600036, Tamil Nadu, India (email: dhiman@iitm.ac.in)

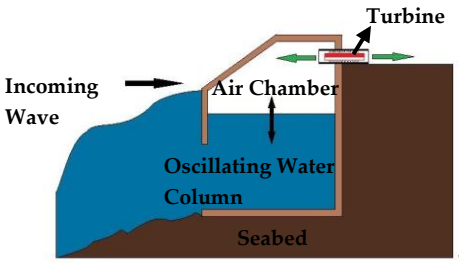

Fig. 1. Oscillating water column.

impulse turbine is one of the types, which has good running characteristics in real ocean conditions [3].

Setoguchi et al. [4] reported that the performance of turbines having self-pitch controlled guide vanes (GVs) was better than the ones with fixed GVs for wave energy impulse turbine. However, these designs reduce the operating life cycle and increase maintenance cost. It has been found that till now various design modifications have been proposed to get the optimal design of an impulse turbine[5], [6]. It has been found that an optimum guide vane angles for maximum efficiency of impulse turbine occur at 30° studied by Maeda et al. [7]. Setoguchi et al. [8] reported that the starting characteristic of impulse turbine does not depend on hub-to-tip ratios and Reynolds number, and found that the optimum hub-to-tip ratio and Reynolds number are 0.7 and 40,000 respectively. Till now various experiments and numerical studies conducted on impulse turbine for different flow conditions such as unsteady, steady and ocean conditions [9].

Endwall contouring is basically providing a curvature surface around the rotor blade at the hub, which is also known as a fillet. The concept of the fillets (linear and variable) has been applied till now on the various gas turbine to reduce the secondary flow losses occurring due to the combined effect of passage vortex, horseshoe vortex and corner vortex. Zess and Thole [10] experimentally and numerically reported that placing of linear fillets of 1δ high and 2δ long at endwall juncture mitigates the strength of horseshoe vortex and reduces the losses. Sung and Lin [11] reported that linear fillets of 1δ, 1.5δ and 2δ have favourable effects in turbine blades in reducing the losses. The experimental investigation concluded by Kubendran and Harvey [12] shows that curved and linear fillets of 0.14δ and 0.28δ have a strong influence in reducing the losses by weakening the effect of vortices. Devenport et al.

[13] reported strake fillet of sizes 4.35 mm, 8.37 mm are effective in reducing the leading edge vortex significantly. Pierce and Shin [14] showed that triangular fillet fence of 0.78δ reduces the turbulent kinetic energy by 10%. Oliver Reutter et al. [15] reported for three different fillets and found that 16% loss reduction. Sauer et al. [16] experimentally reported that bulb on LE of 1.7δ is effectively reducing secondary flow losses. However, to the best of knowledge, the effect of endwall contouring has not been studied on the wave energy harvesting turbine. In this article, a BDI is integrated with the three different endwall contouring (fillets) with heights and steady flow conditions have been analysed and discussed to find out the effect of fillet radius on wave energy impulse turbine for ocean conditions.

II. NUMERICAL METHODOLOGY

A. Reference geometry and modified geometry

This paper presents a numerical analysis of the 0.3 m impulse turbine with 30 RBs and 26 GVs. The reference geometry (Fig. 2) and profile parameters are taken from Setoguchi [8]. The detailed specification and parameters of the reference bidirectional turbine are given in Table I.
Endwall contouring is a turbine blade with fillet and three different fillet radii of 0.54 mm, 1.62 mm and 2.7 mm were taken for the study.

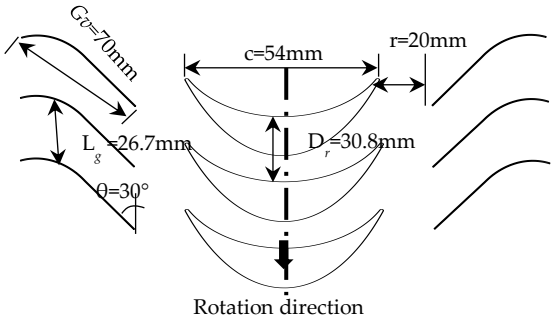

Fig. 2. Reference turbine.

Table I
REFERENCE GEOMETRY PARAMETERS

Design variable	Specifications
Rotor profile	Elliptical-circular
Number of RB	30
RB chord length	54 mm
Rotor-stator axial distance	20 mm
Rotor setting angle	60°
Rotor maximum thickness	16.1 mm
Number of GVs	26
GV profile	Plate type
GV setting angle	30°
GV blade thickness	0.5 mm
GV chord length	70 mm
Hub diameter	210 mm
Tip diameter	298 mm
RB tip clearance	1 mm

Table II
BOUNDARY CONDITIONS

Parameters	Description
Inlet boundary	Axial velocity
Fluid	Ideal gas
Rotor shroud boundary	Moving wall
Flow analysis	Steady state
Turbulence model	K-ω SST
Convergence criteria	1.0E-06
Mesh type	Unstructured(tetra)
Rotor hub, stator hub	No slip wall
Rotational speed	600 rpm
Meshing elements	4 Million
Sidewalls	Periodic boundary
Number of iterations	4000
Outlet boundary	Static pressure(1 atm)

B. Flow analysis under the steady study

The reference 3D geometry (Fig. 3) was modelled, and an unstructured grid was created with prism layer of first cell height of 0.01462 mm from hub to tip of the rotor in Ansys-ICEMCFD (Fig. 4). Ansys-CFX solver was used for steady state turbulent flow simulation, where the finite volume method for solving RANS equations along with the SST turbulence model was utilized. Frozen rotor scheme was used for interfacing the rotor with the stator. The high-resolution numerical scheme, which is nominally second-order accurate and bounded, was utilized for improved numerical accuracy. The computational domain (Fig. 5) of GVs was extended to 8 times of guide vane chord length at upstream and downstream directions with a constant axial distance between rotor and stator. The boundary conditions for numerical study are given in Table II.

The governing equations for the numerical analysis are Reynolds-averaged continuity equation and Reynolds-averaged momentum equation along with the closure model equations.

$$\frac{\partial \rho u_i}{\partial u_j} = 0 \tag{1}$$

$$\rho\left[\frac{\partial \bar{u}_i}{\partial t} + \frac{(\partial \bar{u}_i \partial \bar{u}_j)}{\partial x_j}\right] = -\frac{\partial \bar{p}}{\partial x_i} + \frac{\partial}{\partial x_j}\left[(\mu + \mu_t) + \left(\frac{\partial \overline{u_i}}{\partial x_j}\frac{\partial \bar{u}_j}{\partial x_i}\right)\right] \tag{2}$$

k-ω SST turbulence model equations [17].

$$\frac{\partial(\rho k)}{\partial t} + \frac{\partial(\rho u_j k)}{\partial x_j} = \rho P - \dot{\beta}\rho\omega k + \frac{\partial}{\partial x_j}\left[(A)\frac{\partial k}{\partial x_j}\right] \tag{3}$$

$$\frac{\partial(\rho\omega)}{\partial t} + \frac{\partial(\rho u_j \omega)}{\partial x_j} = B + \frac{\partial}{\partial x_j}\left[(A)\frac{\partial \omega}{\partial x_j}\right] + 2(1 - F_1)\frac{\rho\sigma_d}{\omega}\frac{\partial k}{\partial x_j} \tag{4}$$

where $P = \tau_{ij}\frac{\partial u_i}{\partial x_j}$, $\vartheta_t = \frac{k}{\omega}$, A= $\mu + \sigma_k\frac{\rho k}{\omega}$, $B = \frac{\gamma\omega}{k}P - \beta\rho\omega^2$ and F_1=Blending function.

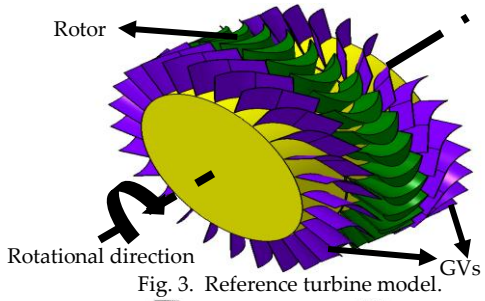

Fig. 3. Reference turbine model.

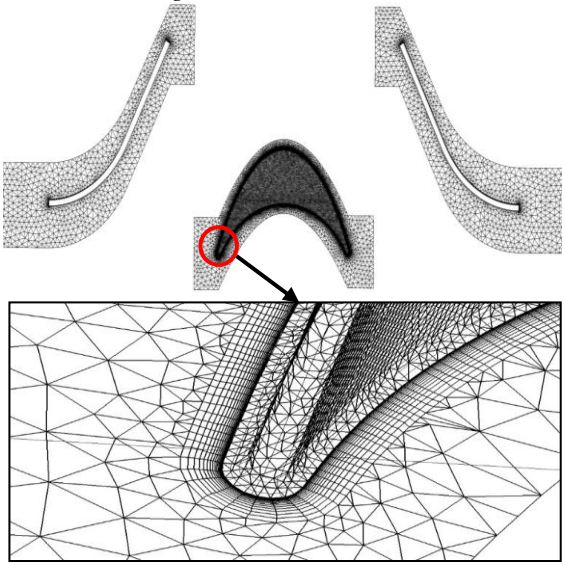

Fig. 4. Computational domain meshing.

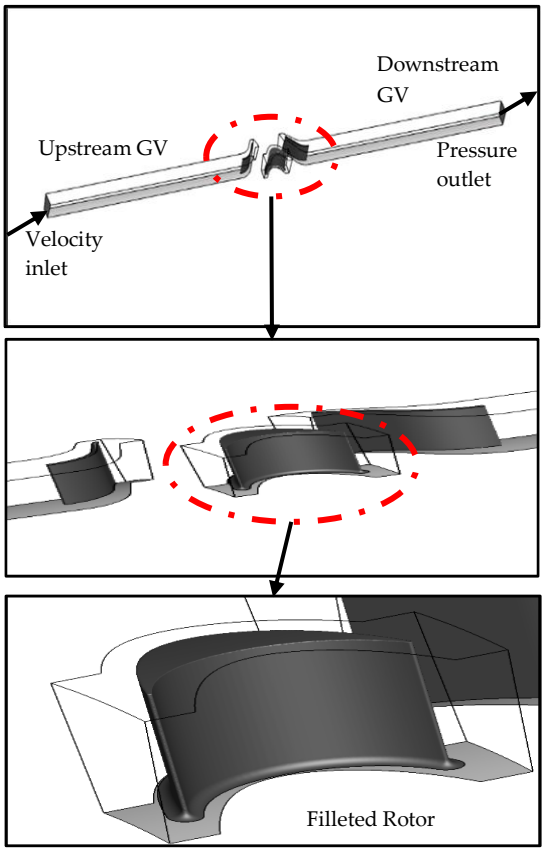

Fig. 5. Computational domain.

III. RESULTS AND DISCUSSION

C. *Grid sensitivity test, steady flow analysis of the reference model and validation*

For the acceptance of any CFD result, grid sensitivity test and validation with existing results are required. Grid sensitivity test (Fig. 6) was carried out for four different grid sizes (1 Million, 2 Million, 4 Million and 8 Million) and found that a good agreement was achieved between 4 and 8 Million cells. Hence, 4 Million cells were taken for numerical analysis. The solution is considered as converged when RMSE value is less than 10^{-6}.

The turbine performance characteristics were calculated and found that 3% error in efficiency (Fig. 7a), 6% and 4.5% in input coefficient (Fig. 7b-7c) and torque coefficient respectively. Thus it may be concluded that the present numerical approach is effective in capturing the performance characteristics of the turbine and hence the underlying flow physics.

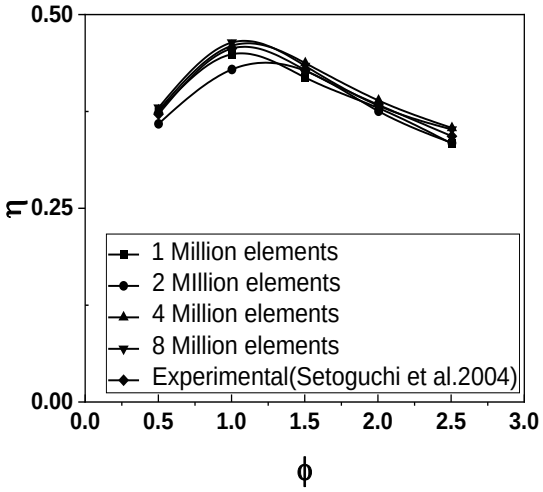

Fig. 6. Grid sensitivity test.

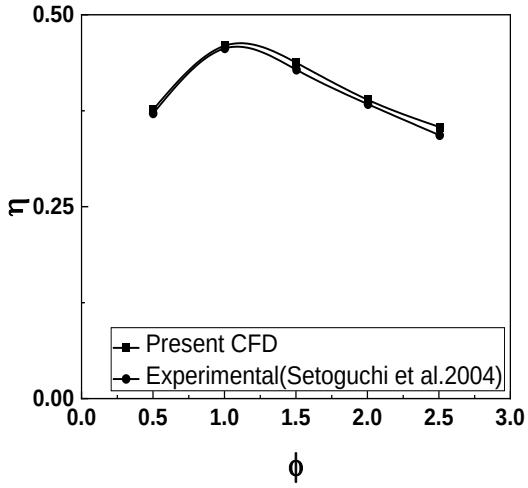

(a) Efficiency vs flow coefficient.

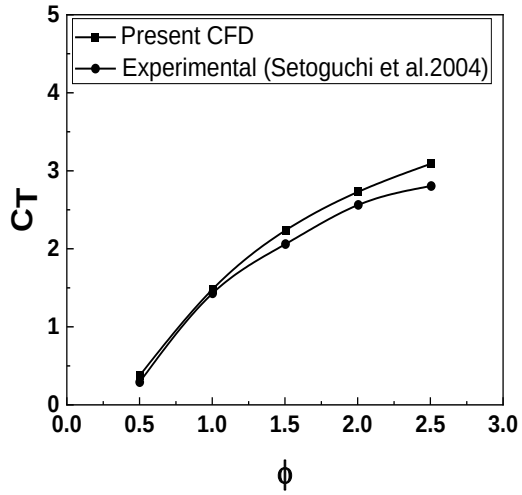

(b) Torque coefficient vs flow coefficient.

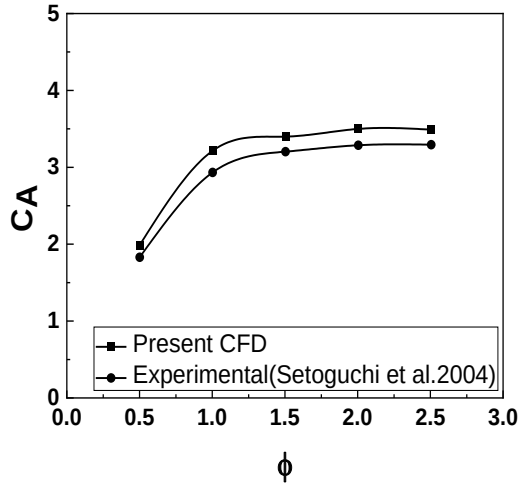

(c) Input coefficient vs flow coefficient.

Fig. 7. Validation of present CFD with experimental results.

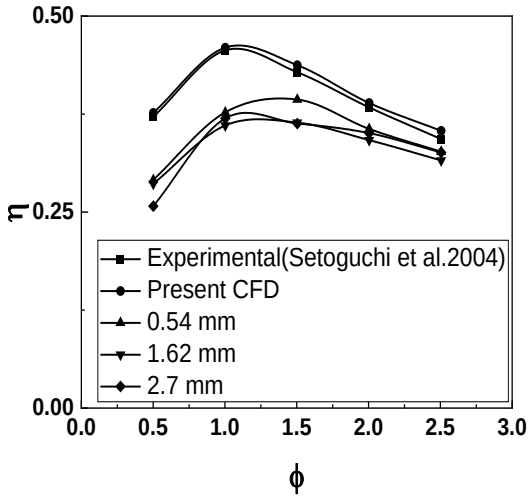

(a) Efficiency vs flow coefficient.

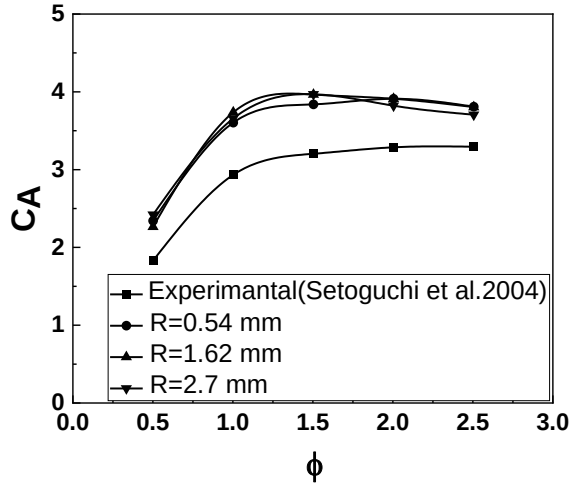

(b) Input coefficient vs flow coefficient.

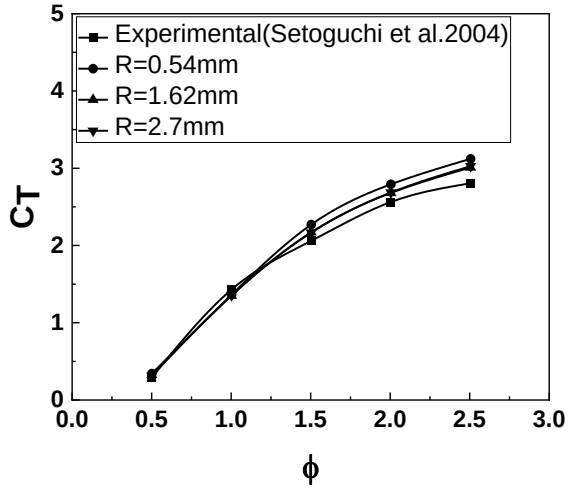

c) Torque coefficient vs flow coefficient.

Fig. 8. Performance characteristics of the filleted rotor.

Equations used for calculating the performance parameter are taken from Setoguchi [8]:

Flow coefficient

$$\phi = \frac{C_a}{U} \tag{4}$$

Torque coefficient

$$C_T = \frac{2T_r}{\rho(C_a{}^2+U^2)sczr_m} \tag{5}$$

Input coefficient

$$C_A = \frac{2\Delta PQ}{\rho(C_a^2+U^2)sczC_a} \tag{6}$$

Efficiency

$$\eta = \frac{C_T}{C_A * \phi} \tag{7}$$

D. Performance characteristics of the filleted turbine

From Fig. 8, it can be observed that integrating the fillet on the rotor affects the overall performance of the turbine. At 0.2% of *s* when fillet radius increases at ϕ=1(Fig.9d), the flow starts separating at 30% of c due to the deacceleration of the fluid particle on PS and SS surface and accelerates towards the exit, which leads to flow separation and mixing at the DGV. Pressure loss due to DGV is the major parameter affecting the efficiency (Fig. 8a) of the turbine by increasing the input flow coefficient (Fig. 8b). The torque coefficient (Fig. 8c) increases at higher flow coefficient while decreases for low coefficients. This leads to an overall decrement in the performance characteristics. As a result, the filleted turbine has less torque compared to the reference turbine. For (R=0.54 mm) fillet has lesser losses compared to the other two radii but more than reference turbine.

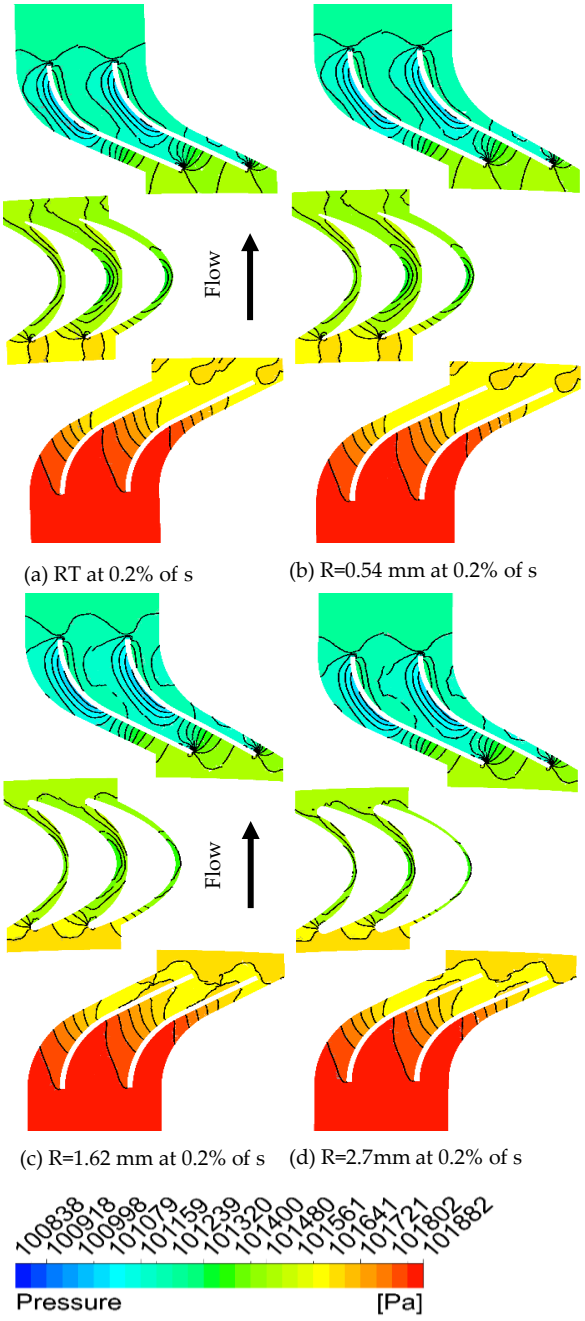

(a) RT at 0.2% of s (b) R=0.54 mm at 0.2% of s

(c) R=1.62 mm at 0.2% of s (d) R=2.7mm at 0.2% of s

Fig. 9. Pressure contours at ϕ=1.

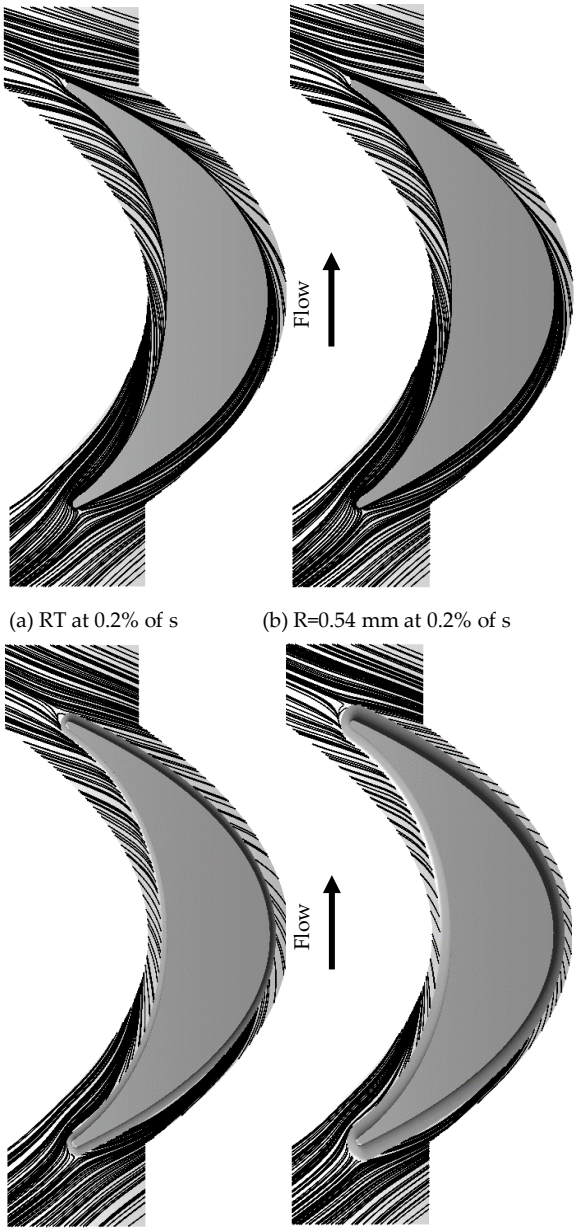

(a) RT at 0.2% of s (b) R=0.54 mm at 0.2% of s

(c) R=1.62 mm at 0.2% of s (d) R=2.7mm at 0.2%of s

Fig. 10. Streamlines at ϕ=1.

E. Flow analysis of filleted turbine

The bidirectional turbine is contoured with the three different types of fillet radii — 0.54 mm, 1.62 mm and 2.7 mm. The fillet radius of more than 2.7 mm cannot be given in the present geometry of the turbine due to space constraint between the periodic and blade surface. It was found that the flow behaviour of the filleted and un-filleted (Reference)[8] turbine are different. Fig. 9 shows pressure contours at 0.2% of *s*. The fillet height is about of 0.2% of *s*, after an investigation of results, it was noticed that at 0.2% of *s*, the flow starts separating on the PS of the rotor at the vicinity of the LE at ϕ = 1. The incoming accelerated flow at ϕ = 1 (R=0.54 mm) from the upstream guide vane (UGV), strikes on the SS of the rotor blade at the vicinity of the LE, the flow near LE has a large negative angle of attack. Therefore, it induces the stall.

The stalled region have flow separation defined as separated flow structures. At ϕ=1, as the flow approaches LE of the rotor, it does not separate from the endwall but rather it deaccelerates near fillet. Vortices begin to grow near the LE of the rotor due to the low-pressure zone created by the flow separation. The flow does not separate near LE at fillet R=2.7 mm (ϕ=1) in comparison to fillet R=0.54 mm and R=1.62 mm radii. Near LE high-pressure zone exists due to the presence of a pressure gradient near LE. The vortices appear and intensify as the flow coefficient is low. At lower flow coefficients flow separation increases as fillet radius is increased but at higher flow coefficients flow starts accelerating on SS in comparison to the reference turbine up to the 50% of c and then slowed down at the exit of the DGV without any significant separation. The work done is obtained due to the difference in peripheral velocity across the rotor. Due to the presence of UVG, the losses got reduced as the peripheral velocity at the outlet section is lesser than the inlet section of the rotor blade. The peripheral velocity is counter-balanced at the exit due to the ambient pressure of 1 atm. The significant pressure drop developed by DGV is the reason for reduction in the performance characteristics of the turbine. Fig.9 illustrates the complete flow physics of pressure contours observed at ϕ=1.

For ϕ=1 at 0.2% of *s*, Figs. 10 shows streamline contours. The flow separation adjacent to LE on SS of the rotor is greater in contrast to reference turbine for fillet radius (R=2.7 mm). Due to the difference in peripheral velocity, as the fillet radius increases the angle of incidence changes accordingly from hub to tip. The flow begins to detach from UGV at 30% of c at higher flow coefficient, which is one of the reasons for the low flow separation on the rotor SS at higher flow coefficients. The flow accelerates at the inlet of the rotor then deaccelerates on the SS of the rotor and accelerates towards the exit, but at higher fillet radius at higher flow coefficients the flow deaccelerates followed by acceleration from 90% of c without any vortices generation.

For ϕ=1 at 0.2% of *s*, Fig. 9 at fillet radius of R=1.62 mm and R=2.7 mm, the flow separation at DGV is larger than fillet radius of R=0.54 mm. The pressure drop between guide vanes for fillet radius of R=1.62 mm and R=2.7 mm is greater than the fillet radius of R=0.54 mm. The incoming flow decelerates at LE of the rotor on PS due formation of the passage flow vortex at low flow coefficients. The vortices split into two parts as incoming boundary layer approaches the LE of the rotor blade and stagnates. One vortex begins to move on PS and another on SS. This happens due to the presence of pitch wise pressure gradient, i.e. vortices from PS moves towards the SS and interaction between the PS vortex to SS vortex, generates the horseshoe vortex, which dominating flow structure till the exit of the rotor.

The flow experiences losses due to the presence of turbulent mixing, wall shear, all these factors are major contributors to the performance of the DGV. Since the flow incidence angle for DGV is not uniform, which increases irregularity in flow and dissipation due to chaotic flow behaviour, which results in a higher pressure drop across the turbine.

IV. CONCLUSION

In this present work, numerical analysis of the rotor blade of BDI having endwall contour with three different radii are summarized as follows:

- Efficiency of the modified turbine is lesser than the reference turbine because of the drastic increase in the pressure drop across the BDI due to presence of losses.
- The presence of the flow losses in the turbine which includes profile loss, tip leakage, endwall and secondary losses influences the performance characteristics as examined from the streamline and pressure contours.
- Input coefficient for turbine having contoured endwall has a large increase in pressure drop in comparison to the reference turbine.
- Torque coefficient of modified and reference turbines show similar values at low flow values but has a large variation at higher values.
- The numerical study was done only for rotor blade contouring, which gives the scope of future study of the guide vane with endwall contouring.

Abbreviations and acronyms

CAD	Computational Aided Designing
CFD	Computational Fluid Dynamics
DGV	Downstream Guide Vane
GVs	Guide Vanes
LE	Leading Edge
OWC	Oscillating Water Column
RBs	Rotor Blades
RMSE	Root Mean Square Error
RT	Reference Turbine
TE	Trailing Edge
UGV	Upstream Guide Vane
G_V	Chord length of GV (mm)
r	Rotor-stator axial distance (mm)
θ	GV setting angle (°)
D_r	Rotor pitch (mm)
R	Fillet radius (mm)
L_g	GV pitch (mm)
C_T	Torque coefficient
C_A	Input flow coefficient
η	Efficiency
z	Number of RBs
k	Turbulent kinetic energy (J)
c	Chord length of the rotor (mm)
r_m	Mean radius (mm)

T_r	The torque produced by the rotor (Nm)
U	Blade velocity (m/s)
C_a	Axial velocity (m/s)
ΔP	The pressure difference between inlet and outlet (N/m^2)
Q	Discharge (m^3/s)
ω	Angular velocity (m/s)
s	Span of RB (mm)

REFERENCES

[1] R. Pelc and R. M. Fujita, "Renewable energy from the ocean," *Mar. Policy*, vol. 26, no. 6, pp. 471–479, 2002.

[2] A. F. O. Falcão and J. C. C. Henriques, "Oscillating-water-column wave energy converters and air turbines: A review," *Renew. Energy*, vol. 85, pp. 1391–1424, Jan. 2016.

[3] M. Takao and T. Setoguchi, "Air turbines for wave energy conversion," *Int. J. Rotating Mach.*, vol. 2012, pp. 1–10, 2012.

[4] T. Setoguichi, K. Kaneko, H. Maeda, T. W. Kim, and M. Inoue, "Impulse turbine with self-pitch-controlled tandem guide vanes for wave power conversion," *Int. J. Offshore Polar Eng.*, vol. 4, no. 1, pp. 76–80, 1994.

[5] K. Ezhilsabareesh, S. H. Rhee, and A. Samad, "Shape optimization of a bidirectional impulse turbine via surrogate models," *Eng. Appl. Comput. Fluid Mech.*, vol. 12, no. 1, pp. 1–12, 2018.

[6] R. Badhurshah and A. Samad, "Multiple surrogate based optimization of a bidirectional impulse turbine for wave energy conversion," *Renew. Energy*, vol. 74, pp. 749–760, Feb. 2015.

[7] H. Maeda, S. Santhakumar, T. Setoguchi, M. Takao, Y. Kinoue, and K. Kaneko, "Performance of an impulse turbine with fixed guide vanes for wave power conversion," *Renew. Energy*, vol. 17, no. 4, pp. 533–547, 1999.

[8] T. Setoguchi, M. Takao, S. Santhakumar, and K. Kaneko, "Study of an impulse turbine for wave power conversion: effects of reynolds number and hub-to-tip ratio on performance," *J. Offshore Mech. Arct. Eng.*, vol. 126, no. 2, p. 137, 2004.

[9] T. Setoguchi, S. Santhakumar, H. Maeda, M. Takao, and K. Kaneko, "A review of impulse turbines for wave energy conversion," *Renew. Energy*, vol. 23, no. 2, pp. 261–292, 2001.

[10] G. A. Zess and K. A. Thole, "Computational design and experimental evaluation of using a leading edge fillet on a gas turbine vane," *J. Turbomach.*, vol. 124, no. 2, p. 167, Dec. 2002.

[11] C.-H. Sung and C.-W. LIN, "Numerical investigation on the effect of fairing on the vortex flows around airfoil/flat-plate junctures," in *26th Aerospace Sciences Meeting*,Reno,Nevada, 1988, pp. 88-0615.

[12] L. Kubendran and W. Harvey, "Juncture flow control using leading-edge fillets," in *3rd Applied Aerodynamics Conference*,Hampton,Virginia, 1985,pp. 85-4097

[13] W. Devenport, R. Simpson, M. Dewitz, and N. Agarwal, "Effects of a strake on the flow past a wing-body junction," in *29th Aerospace Sciences Meeting*,Reno,Nevada, 1991,pp. 091-0252.

[14] F. J. Pierce and J. Shin, "The Development of a turbulent junction vortex system (Data bank contribution)," *J. Fluids Eng.*, vol. 114, no. 4, p. 559, 1992.

[15] O. Reutter, M. Rozanski, A. Hergt, and E. Nicke, "Advanced endwall contouring for loss reduction and outflow homogenization for an optimized compressor cascade," *Int. J. Turbomachinery, Propuls. Power*, vol. 2, no. 1, p. 1, Mar. 2017.

[16] H. Sauer, R. Müller, and K. Vogeler, "Reduction of secondary flow losses in turbine cascades by leading edge modifications at the endwall," *J. Turbomach.*, vol. 123, no. 2, p. 207, 2001.

[17] F. R. Menter, "Two-equation eddy-viscosity turbulence models for engineering applications," *AIAA J.*, vol. 32, no. 8, pp. 1598–1605, 2008.